The atmospheric carbon sequestration potential of man-made tidal lagoons

Piano, Marco; Papadimitriou, Stathys; Roche, Ronan; Bowers, David; Kennedy, David; Kennedy, Hilary

Continental Shelf Research

DOI:
10.1016/j.csr.2019.05.011

Published: 15/06/2019

Peer reviewed version

Continental Shelf Research

The atmospheric carbon sequestration potential of man-made tidal lagoons

Marco Piano[a*], Stathys Papadimitriou[b1], Ronan Roche[a], David Bowers[b], Paul Kennedy[b], Hilary Kennedy[b]

*corresponding author: m.piano@bangor.ac.uk

[a]Centre for Applied Marine Science (CAMS), Bangor University, Menai Bridge, Anglesey, LL59 5AB United Kingdom

[b]School of Ocean Sciences (SOS), Bangor University, Menai Bridge, Anglesey, LL59 5AB United Kingdom

The authors confirm that there are no known conflicts of interest associated with this publication and there has been no significant financial support for this work that could have influenced its outcome.

Abstract

Understanding sequestration of carbon by coastal ecosystems is central to addressing the role they play in climate change mitigation. To quantify this process, accurate measurements of CO_2 fluctuation, coupled with variations in residence time of coastal water-bodies are required. Nearshore ecosystems, including coastal lagoons, may provide an effective sink for atmospheric carbon dioxide, particularly those containing productive biota such as seagrass. However, the rate and pattern of carbon sequestration in seagrass meadows across a range of environmental settings is still poorly constrained. In this study, we utilize a robust physical tidal model, along with biogeochemical dissolved inorganic carbon (DIC) assessment, to estimate water residence time and net sequestration of atmospheric CO_2 in an intertidal lagoon containing a seagrass (*Zostera noltii*) meadow. Total alkalinity and pH measurements taken from advected water mass exchanged with the open ocean at inlet boundaries are used to calculate DIC and pCO_2. A predictive model of hydrodynamics provides good approximation of mean water residence time to within 6 hr (± 3 s.d). Results indicate that during the daytime study period the lagoon is a sink for carbon, having a mean net ecosystem productivity (NEP) of 3.0 ± 0.4 mmol C m^{-2} hr^{-1}. An equivalent diel NEP range of between 15.23 and -9.24 mmol C m^{-2} d^{-1} is calculated based on reported shallow water pelagic respiration rates. Moreover, approximately 4% of DIC availability occurs from atmospheric CO_2 transfer to lagoon water. However, a negative diel rate of -82 ± 81 mmol C m^{-2} d^{-1} is found, assuming overnight respiration ascertained from converted *Zostera noltii* O_2 utilization. We hypothesize that analogous regional

1. Ocean Technology and Engineering, National Oceanography Centre, European Way, Southampton, SO14 3ZH United Kingdom

nearshore ecosystems provide baseline study sites suitable to elucidate the carbon capture potential of planned, nearby tidal range energy schemes.

Keywords

Coastal lagoons; Atmosphere-ocean carbon exchange; Tidal energy; Carbon sinks; Dissolved Inorganic Carbon; Irish Sea coastal modelling

1. Introduction

Coastal lagoons, saline ponds and barrier systems occupy around 13% of coastal areas worldwide and accommodate important productive habitats such as seagrass meadows (Barnes, 1989). Despite their sparse ocean coverage (<0.2%), seagrass meadows play an important role in carbon sequestration and burial, estimated to be between 20 and 112 Tg C yr^{-1} (Duarte et al., 2010; Kennedy et al., 2010; Fourqurean et al., 2012). However, not all seagrass meadows are net autotrophic (Duarte et al., 2010); many nearshore coastal ecosystems are thought to contribute to atmospheric CO_2 levels by acting as a net source, with heterotrophic processes that produce CO_2 outweighing autotrophic processes that consume it (Mork et al., 2016). Coastal lagoons can be productive environments due to high nutrient levels in both sediments and water, and are frequently colonized by benthic plants due to suitable sunlight penetration in the shallow water column. They represent a valuable resource for both fisheries and blue carbon initiatives, supported by research finding that shallow water autotrophic biota provide a functional sink for atmospheric CO_2 (Tokoro et al., 2014).

Current global carbon budgets show a deficit that is unattributed of 0.6 Gt C yr^{-1} (Le Quere et al., 2018). The oceanic sink of anthropogenic CO_2 for the period 2002 to 2011 is estimated at 2.5 ± 0.5 Pg C yr^{-1} (Le Quere et al., 2013), with oceanographers researching understudied parts of the ocean, such as marginal seas and nearshore ecosystems as potential missing sinks. Bauer et al. (2013) and Borges et al. (2005) suggest (with some uncertainty) that temperate marginal seas may reduce atmospheric CO_2 by some 0.45 Pg C yr^{-1}, with nearshore wetland and estuarine ecosystems almost nullifying this sink by emitting around 0.35 to 0.40 Pg C yr^{-1}. It is suggested that future research should focus on increasing high resolution carbonate system parameter data (Mork et al., 2016) in highly productive nearshore systems, such as those containing seagrass (Borges et al., 2005; Dai et al., 2009; Jiang et al., 2011). Tidal range power schemes, such as the proposed Swansea Bay tidal lagoon[A] may provide an opportunity to fabricate carbon-sequestering nearshore ecosystems that increase the potential to offset atmospheric carbon deficits.

[A] http://www.tidallagoonpower.com/projects/swansea-bay/

Roche et al. (2016) suggest that accurate resource assessments relating to marine renewable energy (MRE) schemes are required to elucidate physical, ecological and social uncertainties when spatially refining developments to help achieve carbon reduction targets. Tidal lagoons provide an important potential resource for the MRE development mix, being both a predictable and controllable renewable energy source. The feasibility and scope of planned UK tidal lagoon energy schemes has undergone extensive examination by the 'Hendry Review'. However, uncertainty exists as to their future, given the high initial capital costs involved and possible inability to produce electricity at a competitive price. Additional benefits, such as regeneration, recreational activities and flood protection are suggested (Neill et al., 2018; NIC, 2018), however, the opportunity to incorporate carbon offsetting might also provide a second potential revenue source, increasing financial feasibility.

A naturally restricted lagoon is defined as having two or more frictional inlets, with definite tidal regimes, whereas choked lagoons characteristically have one or more long narrow inlets with greater water residence time (Kjerfve, 1986). Residence time is a quantitative measure allowing spatial and temporal estimation of the rate at which water mass ingresses and egresses a control domain. It is effectively the time taken for a particle entering the domain to leave again for the first time (Delhez et al., 2014). Ecosystem issues such as depletion in fish production have been related to limited seawater circulation and renewal (Tsihrintzis et al., 2007), because flushing has a limiting impact on nutrient input (Newton and Mudge, 2005). Salt concentration, along with nutrient and alkalinity balance may be reduced by inputs of freshwater from surface run-off, contributories, heavy and prolonged precipitation or by evaporation. It should be noted that larger lagoon systems are characteristically more stable and likely to encourage species diversity (Barnes, 1989). Ultimately, water balance, composition and quality depends on exchange at boundaries and the resultant residence time (Orfila et al., 2005; Rynne et al., 2016).

Coastal lagoons are important areas for autotrophic processes resulting in net carbon accumulation in sediments but are susceptible to anthropogenic impacts. Industrial activities such as fossil fuel combustion and cement manufacturing have increased atmospheric CO_2 concentration, influencing water pH. Terrestrial deforestation and habitat clearing have created aquatic imbalances known as cultural eutrophication and siltation, often manifested by increased turbidity, algal production, decreased light availability and dissolved oxygen levels (Kennedy and Bjork, 2009; Zouiten et al., 2013). Ultimately, this may cause loss of benthic plants and oxidation of sediments leading to net heterotrophic activity, causing the lagoon to act as a carbon source rather than a sink. It is, therefore, important to be able to robustly model carbon dynamics in order to assess whether ecosystems are CO_2 sources or sinks.

In this study, we provide a method to quantify simply and robustly mean lagoon NEP rates based on observed boundary flux estimates of DIC and modelled water exchange through the tidal channels. The study site has restricted water exchange with the open ocean through man-made inlets and is located in the vicinity of proposed sites for tidal lagoon power schemes that will follow similar water exchange regimes. As such similar regional ecosystems may provide analogous baseline study sites for proposed MRE schemes. A physical-chemical box model approach provides volumetric water exchange estimates at lateral boundaries from simulations provided by a one-dimensional (1-D) MATLAB model. Modelled hydrodynamics are well validated; thus, errors are constrained. Biogeochemical field measurements along with meteorological data allow air-sea CO_2 transfer rates to be estimated over a complete tidal cycle. This short-term study demonstrates the utility of this approach and identifies the potential for annual carbon budgeting in semi-enclosed productive coastal lagoons using high-resolution temporal data.

2. Methods

2.1 Study site

Sampling occurred in the Inland Sea (53°16.475'N, 4°35.000'W), a small (radius and surface area at low tide ~890 m and 2.5 km^2, respectively), shallow (~2 m at low tide), temperate, micro-tidal (<2 m range) coastal lagoon. The nearshore ecosystem is sandwiched between road and rail embankments in a channel that separates Holy Island from the island of Anglesey in Wales, UK (Figure 1). The lagoon was formed in the early 19th century when Stanley Embankment (water inlet ~17 m wide and 100 m long) was constructed to provide a transport route through to Holyhead. At the opposite end of the lagoon, Four Mile Bridge provides a much narrower road bridge and passage for water to enter (~6 m wide by 10 m long). The area is both a designated Landscape Character Area (LCA) and Area of Outstanding Natural Beauty (AONB) and provides an important well-balanced nursery and ecosystem for many different fish and marine plant species. Further detail on the area is provided by Hill (1994).

Seawater exchange with the Irish Sea occurs through the two narrow man-made inlets in the embankments. The hydrodynamic regime of the lagoon is dominated by semi-diurnal advective mixing of seawater at lateral boundaries. Periodic tidal forcing outside the basin is choked by the restricted inlets so that the tide in the Inland Sea has a lower amplitude than that of the open ocean (Hill, 1994). The lagoon supports a meadow of *Zostera noltii*, a small seagrass species of the intertidal zone of Europe and Africa (Auby and Labourg, 1996). This species exhibits strong seasonality in its above-ground biomass, ranging from 0.4 g DW m^{-2} in spring to 70 g DW m^{-2} in summer (Papadimitriou et al., 2006). There are a number of proposed MRE

developments for this region, including a tidal range lagoon scheme to the east at Colwyn Bay (Roche et al., 2016).

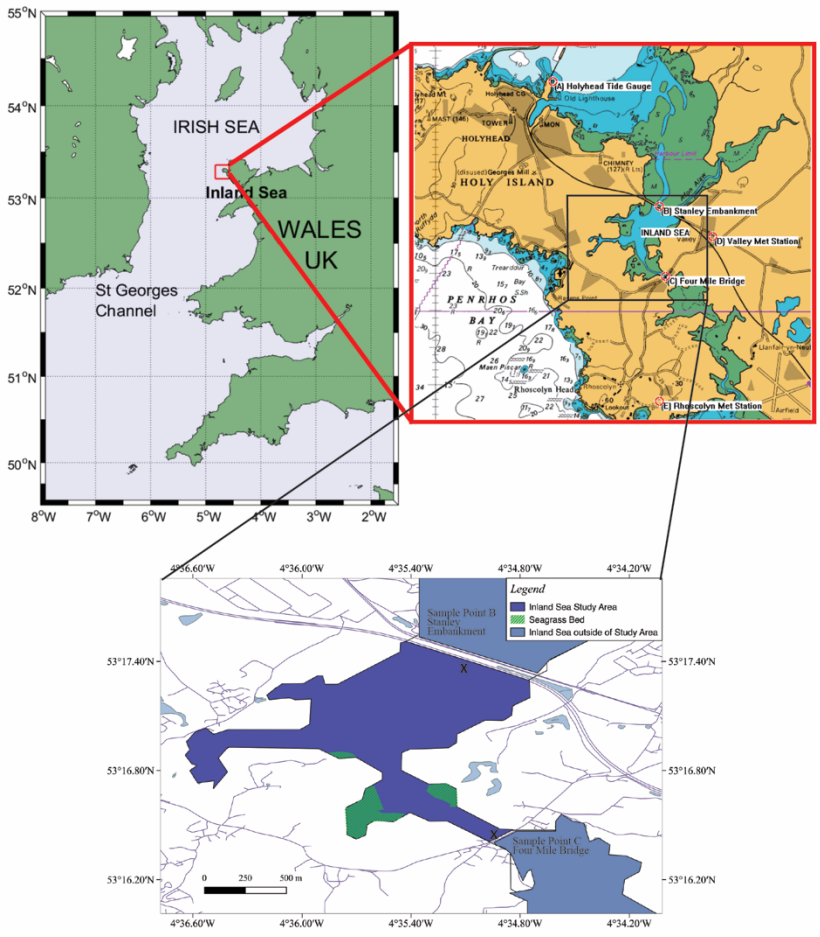

Figure 1. Location of the Inland Sea showing the restricted channels to the north at Stanley Embankment (B) and to the south at Four Mile Bridge (C). Modelled boundary conditions are based on data supplied by Holyhead harbour primary tide gauge station (A) and meteorological data is taken from stations at Valley (D) and Rhoscolyn (E).

2.2 Biogeochemical model

A simple theoretical 1-D biogeochemical model, adapted from Jiang et al. (2011) (Figure 2) is used to examine the extent to which lagoon DIC concentration is influenced by CO_2 gas exchange caused by a combination of:

(i) air-sea exchange (surface boundary)

(ii) physical mixing (lateral boundary)

(iii) biological influences (seabed and water column)

DIC determination is outlined in section 2.4. We apply the fundamental principles of a tracer (in this case DIC) entering and exiting a semi-enclosed system and assume (a) lagoon volume is conserved and (b) a fully mixed water column. Therefore, tracer concentration (c, in mmol C kg^{-1}) in a varying water depth over time is given by eq (1) (Williams and Fellows, 2011):

$$\frac{d}{dt}\rho c\frac{V}{A_S} = \sum F_{out} - F_{in} = F_{MIX} - F_{GAS} - F_{BIO} \quad (1)$$

In the above equation, ρ is water density (kg m^{-3}), V system volume (m^3), A_S surface area (m^2), and F is the tracer flux (mmol C m^{-2} hr^{-1}) entering (F_{in}) and exiting (F_{out}) the system at the boundaries. DIC fluxes in and out of the lagoon can further be expressed as the sum of the partial fluxes generated by a number of biogeochemical processes within the lagoon:

(i) Physical mixing during transport by advection over ebb and flood tidal cycles, riverine input, and upwelling (F_{MIX}).

(ii) Ecosystem respiration, adding respired organic carbon as CO_2 to the water, and ecosystem production removing DIC species (aqueous CO_2, bicarbonate ions) from the water into biomass and calcium carbonate ($CaCO_3$) precipitation and dissolution, combined as F_{BIO}.

(iii) Air-sea exchange of CO_2 (F_{GAS}). If $F_{in} > F_{out}$, there will be a net increase in DIC concentration in the lagoon water, and vice versa.

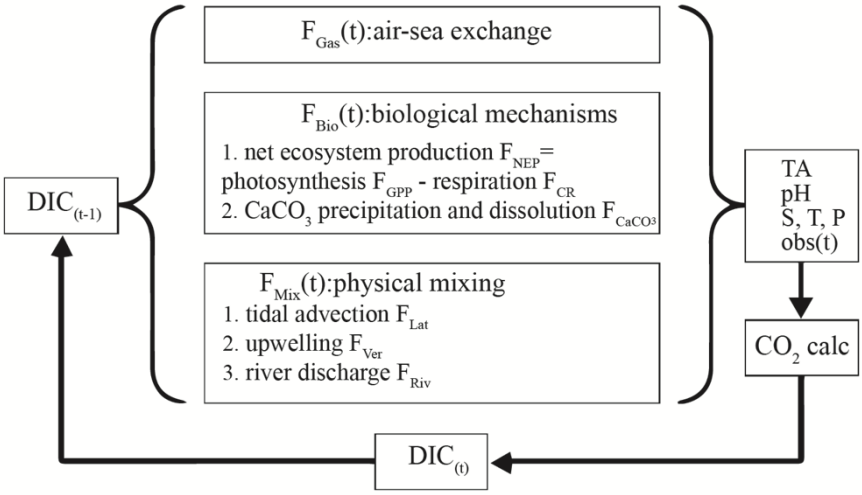

Figure 2. Biogeochemical 1-D model of carbonate system exchange dynamics when accounting for associated air-sea gas exchange, biological activity and physical processes in a nearshore shallow water ecosystem.

2.2.1 Biological processes

We simplify the approach to carbon dynamics in the lagoon by considering a semi-enclosed system (Figure 3). At first approximation, we assume that the contribution from $CaCO_3$ precipitation and dissolution is negligible (Barron et al., 2006). Based on eq (1), at steady state F_{BIO} is equivalent to NEP, the balance between gross primary production and community respiration, F_{BIO} = NEP = GPP + CR. By

convention, the transfer of carbon from atmosphere to seawater and lagoon to ocean due to respiration have negative values.

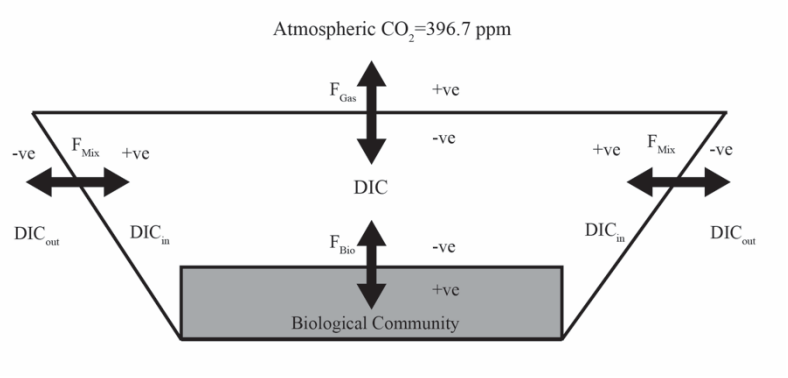

Figure 3. Schematic box model of the Inland Sea and its perceived inorganic carbon exchange. Lateral tidal mixing (Mix), biological (Bio) and gas (Gas) exchanges will drive net DIC concentration levels within the lagoon.

2.2.2 Air-sea exchange

In this study, we determine F_{GAS} with the bulk formula method as $F_{GAS} = \alpha k \Delta pCO_2$. Where α is the solubility coefficient of CO_2 (mmol m^{-3} μatm^{-1}), k is gas transfer velocity (m hr^{-1}; a function of wind speed) and $\Delta pCO_2 = pCO_{2W} - pCO_{2A}$ (µatm), the air-sea difference in the partial pressure of CO_2. Subscripts *W* and *A* refer to water and atmosphere respectively.

2.2.3 Physical mixing

By observing any two of the four measurable carbonate system parameters, pH, DIC, total alkalinity (TA) and pCO_2, along with water temperature and salinity, it is possible to determine the remaining parameters. In this study, DIC in lagoon water is determined from field observations of pH and TA at lateral boundaries. The physical processes of tidal advection, upwelling, and river discharge contribute to DIC mixing at ecosystem boundaries. Advection of nutrients from ocean tides dominate the Inland Sea, no other significant contributories exist. The tidal exchange of water through the man-made inlets provides fluxes calculated from the product of volumetric flow throughput, U (m^3 hr^{-1}) and water density. The mixing of lagoon and ocean water includes tracer concentration, such that $F_{MIX} = c_L \rho U_{out} - c_O \rho U_{in}$ whereby subscripts *in* and *out* describe exchange on flood and ebb tides and subscripts *L* and *O* indicate lagoon and ocean concentrations, respectively.

2.3 Hydrodynamic model

The hydrodynamic model provides a means to estimate volumetric channel throughput, *U*. Following Hill (1994), the tide in the Inland Sea is modelled by

considering the balance between the pressure gradient force caused by the slope of the water surface and bottom friction:

$$g\frac{\eta_O - \eta_L}{L} = k_D \frac{u^2}{H + \eta_m} \quad (2)$$

Where g is the gravitational acceleration constant (9.81 m s^{-2}), η_o is surface elevation relative to mean sea level in the open sea (m), and η_L is surface elevation relative to mean sea level in the lagoon (m). The depth-averaged along-channel current velocity u (m s^{-1}, positive when flow is into the lagoon), and k_D the dimensionless drag coefficient in a channel of length L and depth H below mean sea level (m). Mean surface elevation in the channel is denoted by $\eta_m = (\eta_O + \eta_L) / 2$. The continuity equation is:

$$A_S \frac{d\eta_L}{dt} = ub(H + \eta_m) \quad (3)$$

and we consider ideal channels of width b (m), whose cross section does not alter. Crucially, however, in addition we allow the surface area of the lagoon to change with the tide, assuming the lagoon has sloping sides and a conical shape. If the sides slope at an angle θ (°) to the horizontal, the surface area of the lagoon varies with elevation according to:

$$A_S = \pi\left(r_0 + \frac{\eta_L}{\tan\theta}\right)^2 \quad (4)$$

The subtidal lagoon radius, r_o (m) is that at lowest-tide, assumed constant with depth beyond this.

Tidal forcing in the open sea can be represented by a sum of harmonics:

$$\eta_O = \sum_{n=1}^{N} a_n \cos(\omega_n t - \kappa_n) \quad (5)$$

Where a_n and κ_n are the amplitude (m) and phase (°) of n (1-N) tidal constituents with an angular frequency $\omega_n = \frac{2\pi}{T_n}$ with T_n being the period (s) of the constituent. For this study, twelve of the main harmonic constituents are used to represent surface elevation change due to astronomical forcing. Tidal boundary forcing at the Inland Sea

is assumed to occur at the same phase and amplitude as that at Holyhead harbour (A in Figure 1). The flow in the channels is derived by solving eq (2) for *u* and then using eq (3) to update the elevation in the Inland Sea. The equations are solved using a thirty-second-time step with meteorological influences neglected. *U* is derived from the product of channel flow velocity and cross-sectional area, which varies with depth over time.

2.4 Water residence time and NEP

Water exchange and mixing through the channels will not occur instantly and concentrations due to mixing will alter slowly and be affected by a proportion of water returning into the domain soon after leaving. Therefore, the average residence time of the water must be factored into calculations. In order to account for this mixing process, we approach the problem using the tracer pulse method that associates the residence time (T) of a system (in this case the lagoon basin) with n measured tracer flux concentration observations (F_{tr}) at any given point on the periphery during an elapsed time (t) by means of the transport equation:

$$T = \frac{\sum_{n=0}^{\infty} F_{tr} t}{\sum_{n=0}^{\infty} F_{tr}} \tag{6}$$

We solve the steady state condition of eq (6) by integrating over time the multiple tracer DIC flux observations to reveal the solution to tracer transport for a time step equal to a tidal cycle:

$$NEP = \frac{1}{T_{TC}} \int_{0}^{TC} F_{MIX} - F_{GAS}\, dt \tag{7}$$

Water residence time during a tidal cycle (T_{TC}) is the ratio of the mean volume of the lagoon V_L, (m^3) to the tidal prism volume, V_{TP}, ($m^3\ hr^{-1}$) which is the difference between high and low tide volumes or throughput in the channel(s) over an ebb tide (Sheldon and Alber, 2006). For an implicit timescale of a tidal cycle, V_{TP} represents the volume change or throughput over the tidal period, T_{TC}.

$$T_{TC} = \frac{V_L}{V_{TP}} = \frac{\overline{V}}{\Delta V / T_{TC}} \tag{8}$$

In the above equation, the overbar represents the integrated mean values of the polynomial curve fit. We assume negligible difference in concentration values at each lagoon entrance at all times.

3. Applied theory

3.1 Measurements and Analysis

Sampling was conducted in surface waters in daylight hours during an ebb tide pilot study on 1 August 2013 (JD 213) and over a complete tidal cycle during spring tide on 20 August 2013 (JD 232) within a 20 m radius of the culvert entrances at Four Mile Bridge and Stanley Embankment (Figure 1). No precipitation occurred during this time. Single-point current velocity measurements were taken in triplicate at 10- or 15-minute intervals at channel inlets during ebb tides throughout July and August using a Braystoke BFM002 miniature current flow meter. Combined half hour moving averages of these measurements were used to validate model estimates (section 3.2). Solar irradiance was determined from hourly moving averages of data supplied by the observatory at Hilbre Island (53º22.980'N, 3º13.680'W) and is used to support evidence of thermal changes in the lagoon.

The seawater DIC concentration, partial pressure of CO_2 in seawater (pCO_{2W}) and hence the air-sea CO_2 transfer rate (F_{GAS}), were all computed from temperature, practical salinity, TA, and pH measurements using CO2Calc version 1.2.0 (Robbins et al., 2010). Parameters were determined by setting the seawater pH scale using the Dickson and Millero (1987) re-fit of the Mehrbach et al. (1973) stoichiometric dissociation constants of dissolved CO_2, the stoichiometric dissociation constant of HSO_4^- (K_{HSO4}) in Dickson (1990), the total boron concentration in Lee et al. (2010) and air-sea transfer rate parameters of Wanninkhof (1992). Combined hourly moving averages of wind velocity data provided from meteorological stations at Valley (53º16.980'N, 4º33.780'W, 9 m elevation) and Rhoscolyn (53º14.760'N, 4º34.980'W, 13 m elevation) on Anglesey were included to calculate gas transfer velocity (k), in order to estimate the air-sea CO_2 flux also (section 2.2.2). The global average for atmospheric CO_2 concentration (396.7 ppm, NOAA, 2013) was utilized in all calculations of the air-sea pCO_2 gradient necessary for the computation of the air-sea CO_2 transfer rate, as local values are not available nor were in-situ values recorded.

Salinity was measured in sub-samples in the laboratory at ambient temperature (18 - 22ºC) using a portable conductivity meter (WTW Cond 3110) with a WTW Tetracon 325 probe. TA was determined within four days of collection from refrigerated, unfiltered, un-poisoned seawater samples stored in 500 mL borosilicate bottles with ground-glass stoppers sealed with vacuum grease (Apiezon M). The TA

311 analysis was conducted by potentiometric titration with HCl of sample aliquots of
312 known weight at constant temperature in a jacketed vessel using a Metrohm Titrando
313 888 unit. The automatic burette, pH meter, Pt temperature probe, Ag/AgCl/KCl
314 reference electrode, and glass electrode were calibrated with buffers traceable to SRM
315 from NIST and PTB (Merck, pH 2.00, 4.01, 7.00, 9.00 and 10.00 at 25ºC). Daily
316 duplicate potentiometric titrations of CRMs yielded 2227.70 ± 0.68 μmol kg^{-1} for Batch
317 #102 (n = 19, certified TA = 2227.46 ± 0.67 μmol kg^{-1}) and 2221.22 ± 1.44 μmol kg^{-1}
318 for Batch #112 (n = 6, certified TA = 2223.26 ± 0.89 μmol kg^{-1}). The coefficient of
319 variation as relative standard deviation for TA was better than 0.2%.
320 A combined glass electrode and temperature probe (Inlab, 0.1°C resolution)
321 coupled to a portable Mettler Toledo SG2 (MT+2) pH meter were used for seawater
322 temperature and pH measurements. The Inlab combination electrode was calibrated
323 using the buffers described above in a jacketed vessel at constant temperature every
324 2°C from 5 to 20°C and at 25°C. Linear regression of electrode-buffer potential E (in
325 mV) versus NIST buffer pH yielded the electrode-specific apparent standard potential
326 (E_o) and potentiometric slope as a function of temperature (Figure 4a). The
327 potentiometric slope deviated by 1.2% from ideal electrochemical behavior as
328 expressed by the Nernst slope in the temperature range of 10 to 25°C.
329 The E_o and potentiometric slope temperature functions were used to compute
330 seawater pH on the NIST scale from the in-situ electrode-seawater E and temperature
331 measured at 15-minute intervals by immersing the electrode in the main water mass for
332 a period of no less than 120 s. The MT+2 pH meter offered 1 mV resolution, equivalent
333 to 0.02 pH unit measurement uncertainty. The seawater pH on the seawater scale
334 (pH_{SWS}) was determined from pH_{NIST} as $pH_{SWS} = pH_{NIST} + \log(f_{H+})$, with f_{H+} equal to the
335 apparent proton activity coefficient determined at the in-situ salinity as a function of
336 temperature by potentiometric titration (outlined above) as described in Gleitz et al.
337 (1995). For this purpose, the Inlab electrode was coupled to the Metrohm titration
338 system, and Inland Sea water was titrated for TA in triplicate every 5°C from 10°C to
339 25°C. The f_{H+} exhibited a linear temperature dependency at S = 34.9 of the seawater
340 sample (Figure 4b).
341

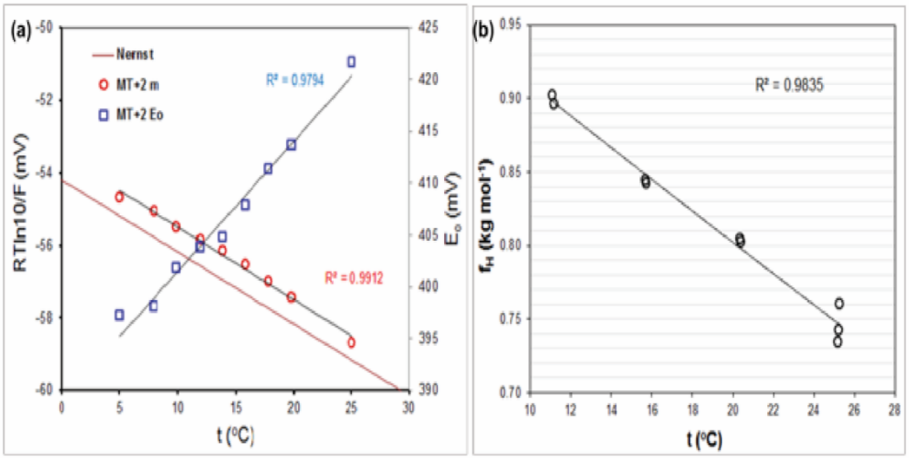

Figure 4. (a) Measured and ideal (Nernst) potentiometric slope (*RTln10/F*) and apparent standard potential (E_o) as a function of temperature of the Mettler Toledo Inlab combination pH-temperature probe using NIST buffer solutions. (b) Apparent proton activity coefficient (f_{H+}) as a function of temperature at S = 34.9 in seawater. The straight lines through the data represent linear regression fits.

342

343 **3.2 Hydrodynamic model validation**

344 Thirty-minute moving averages of single point flow measurements during ebb
345 tide through both channels of the Inland Sea compare well against model outputs
346 (Figure 5). Mean (± 1 s.d) channel velocities of 1.65 ± 0.10 m s^{-1} (n = 14), 1.74 ± 0.18
347 m s^{-1} (n = 11), and 1.02 ± 0.04 m s^{-1} (n = 10) were recorded using the flow meter on 17
348 July 2013 (JD 198), 19 July 2013 (JD 200), and 1 August 2013 (JD 213), respectively.
349 Simulated model outputs for the same periods provided 1.37 ± 0.12 m s^{-1} (n = 64), 1.66
350 ± 0.06 m s^{-1} (n = 45), and 1.05 ± 0.05 m s^{-1} (n = 44).

351

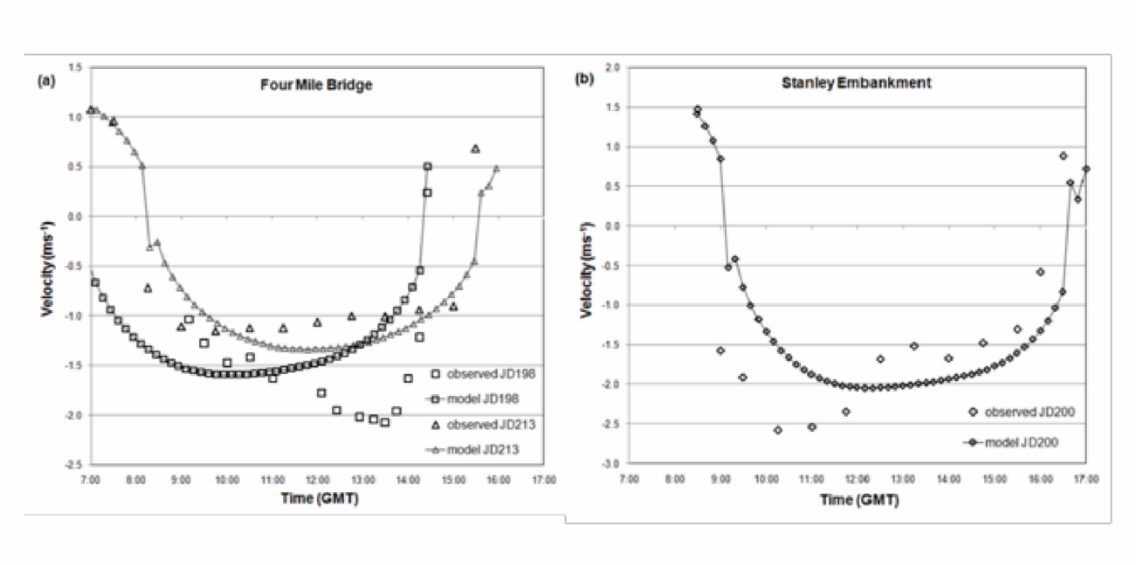

Figure 5. Modelled and observed channel currents. Negative values denote water ebbing away from the lagoon as it empties. Observations were made at culvert entrances to the lagoon at (a) Four Mile Bridge and (b) Stanley Embankment.

352

Modelled boundary tidal forcing, expressed as ocean elevation and phase change at Holyhead (degrees converted to decimal days to provide comparison continuity) for 1 July 2013 (JD 182) to 31 August 2013 (JD 243) inclusive are compared to values published by EasyTide, having decimeter resolution (Figure 6). Mean (± 1 s.d) variation in modelled ocean surface elevation above chart datum (ACD) against published values is 9.5 ± 0.4 cm and the mean variation in phase 1.74° ± 0.07° equivalent to 0.06 ± 2.4x10^{-3} hr (n = 239). Field observations of high and low water times within the Inland Sea are used to validate modelled lagoon phase dynamics (Table 1). These compare well to model predictions; the mean deviation of the modelled lagoon phase is 3.06° ± 2.50 ° or 0.11 ± 0.09 hr (n = 9). Tidal range within the lagoon was also recorded on various days during the study, these observations deviated from modelled lagoon elevation by 2.0 ± 0.7 cm (n = 4). Modelled lagoon surface area minimum and maximum values of 2.43 km^2 and 6.50 km^2 were estimated for the period.

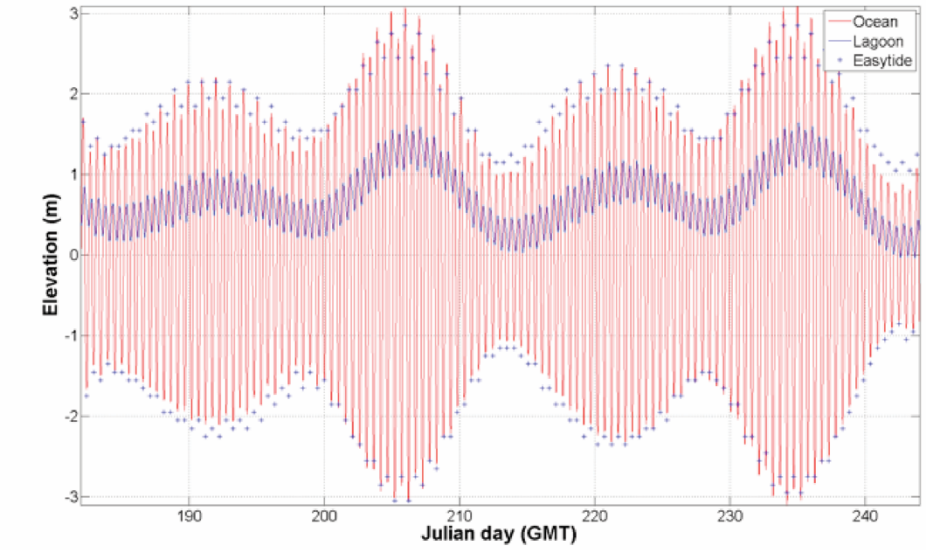

Figure 6. Modelled boundary forcing (red line) based on tidal harmonics at Holyhead compared to published EasyTide data (blue crosses). Simulated lagoon elevation change (blue line) is also plotted.

Table 1 Observations of lagoon high and low water times used to validate modelled lagoon tidal phase and range.

Lagoon tidal phase (hh:mm GMT)		
observed	**model**	**error**
JD192 09:37	09:45	+00:08
JD198 14:20	14:12	-00:08
JD200 08:47	08:49	+00:02
JD200 16:15	16:26	+00:11
JD213 07:56	07:59	+00:03
JD213 15:19	15:20	+00:01

JD232 06:57	07:02	+00:05
JD232 11:25	11:23	-00:02
JD232 18:52	19:09	+00:17

Lagoon tidal range (m)		
JD200 0.45	0.46	+0.01
JD213 0.42	0.43	+0.01
JD232 0.49	0.47	-0.02
JD232 0.46	0.50	+0.04

372

373 **4. Results**

374 Mass balance of DIC is controlled by a combination of physical and biological
375 processes. These include temperature change, water mixing, photosynthetic
376 production of organic material, respiration of marine biota, calcium carbonate
377 precipitation and dissolution, and air-sea transfer of CO_2 across the surface boundary
378 layer. Photosynthesis, $CaCO_3$ precipitation and CO_2 evasion all consume DIC, while
379 respiration, $CaCO_3$ dissolution and CO_2 transfer from atmosphere recycle carbon back
380 into the DIC pool from the organic, mineral and gaseous phases, respectively
381 (Papadimitriou et al., 2012). An imbalance, therefore, in the sinks and sources of DIC
382 will result in a net change in the DIC concentration in an aquatic system.

383 During these processes, the marine CO_2 system will re-equilibrate, with
384 consequent changes in parameters such as pH and the pCO_{2W} of the system. The
385 change in DIC concentrations derived from the empirical observations in this study are
386 considered to be the result of influence from some, or all, of the processes of gas
387 exchange, advection and net ecosystem productivity, leading to a net deficit or excess
388 in the balance between fluxes entering and leaving the lagoon. By capturing the carbon
389 exchange rate at ecosystem boundaries, overall assessment of the net balance
390 between these processes is achieved. Our resultant analysis indicates whether the
391 ecosystem acts to balance the carbon budget as a net sink or source during the study
392 period.

393

394 **4.1 Lagoon system**

395 Changes in lagoon water parameters were observed from 08.00 to 19.30 BST,
396 during a complete spring tidal cycle. The mean lagoon water residence time is
397 estimated at 39 ± 6 hr calculated from simulated model channel throughput values
398 (Table 2). Seawater temperature increased linearly from 16.6°C to 19.8°C over the
399 course of the day, reaching a plateau during mid-afternoon while salinity remained
400 relatively constant at 34.01 ± 0.02 (±1 s.d, n = 24). During the flood period, the pH_{sws}
401 varied between 8.05 and 8.13, while during the ebb tide it increased systematically
402 from 8.05 to 8.26. Total alkalinity initially decreased during flood tide from 2329 µmol
403 kg^{-1} to 2300 µmol kg^{-1} and remained relatively constant for most of the ebb tide, with a

404 small step change of ~10 µmol kg^{-1} toward the end of the study period. The calculated
405 DIC and pCO_{2W} exhibited similar behaviour with sinusoidal fluctuations. During the
406 flood tide, the DIC exhibited a short initial increase followed by a sustained systematic
407 decrease from 2092 to 1937 µmol kg^{-1}. Over the same period, the pCO_{2W} fluctuated
408 between 312 µatm and 394 µatm during flood and exhibited a systematic decrease
409 from 330 µatm to 220 µatm during ebb (Figures 7 and 8; Table 3).
410 The pCO_{2W} indicates that, throughout the study period, CO_2 levels in the lagoon
411 were conducive to transfer of CO_2 from the atmosphere to seawater. Wind velocity
412 increased over the course of the day from 1.6 m s^{-1} at the start of the study to almost 5
413 m s^{-1} by the end (Figure 8). The F_{GAS} calculations were estimated to be negative
414 throughout the study period (Figure 9), indicating again that the air-sea exchange of
415 CO_2 occurred from atmosphere to seawater. There was an increase from a minimum
416 air-sea flux of –0.002 mmol C m^{-2} hr^{-1} to a maximum of –0.38 mmol C m^{-2} hr^{-1}, with a
417 mean (± 1 s.d) F_{GAS} = –0.13 ± 0.26 mmol m^{-2} hr^{-1}. The mean NEP rate for this tidal
418 period Is estimated at 3.0 ± 0.4 mmol C m^{-2} hr^{-1} (Table 3), with F_{GAS} equivalent to 4.3%
419 of NEP DIC provision.
420
421 **Table 2** Calculated water residence time based on cumulative modeled channel flow data over
422 the mean ebb and flood period during sampling.
423

	Flood (m^3 hr^{-1})	**Ebb (m^3 hr^{-1})**	**Water Residence Time (hr)**
Min	3032258	1098513	33.4
Max	3057142	823390	45.0
Mean Period (hr)	4.5	7.6	

424

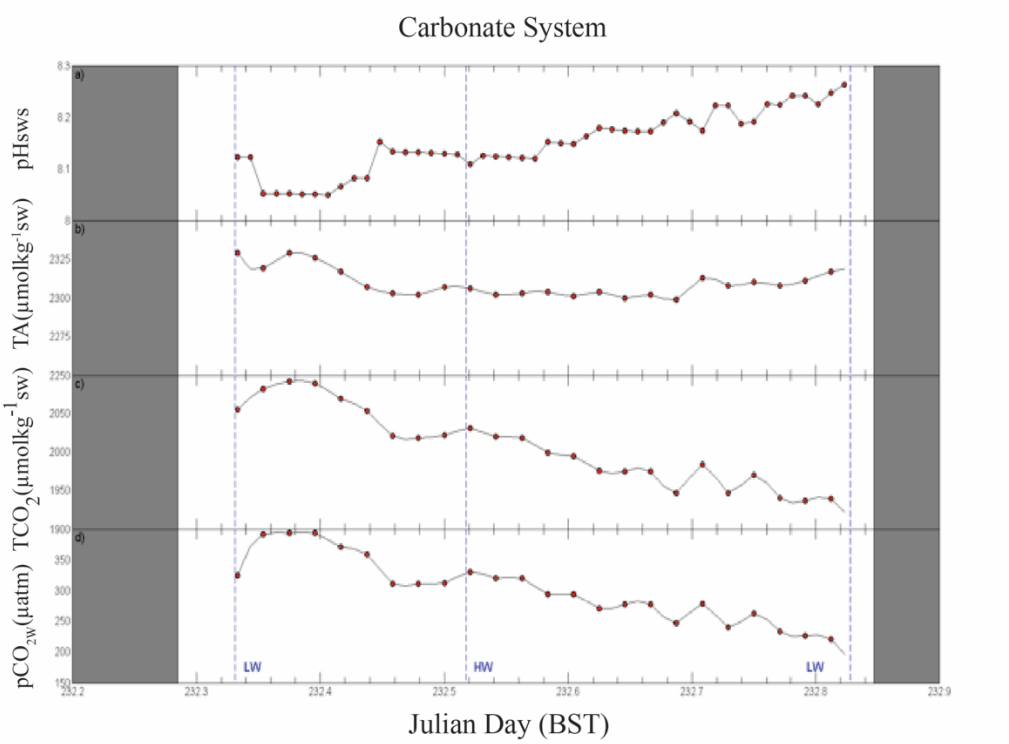

Figure 7. Lagoon carbonate system parameters of (a) pH (b) TA (c) DIC and (d) pCO_2 on JD 232 (solid markers). DIC and pCO_2 are derived from CO2Calc estimates of in-situ pH and TA observations. High and low water (blue lines) and non-daylight hours (grey areas) are also indicated.

425

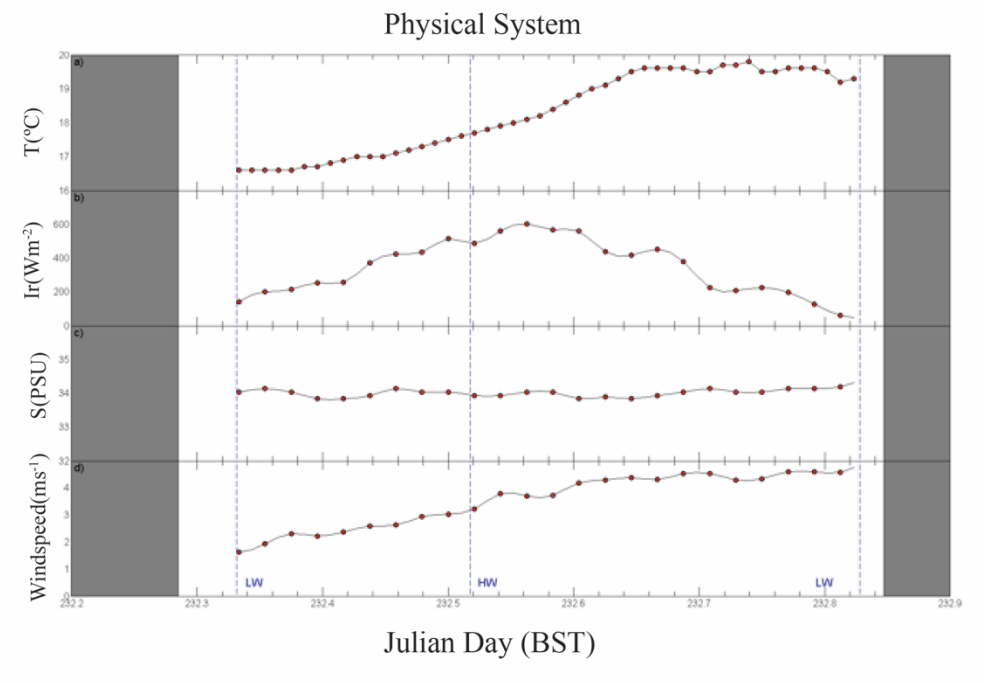

Figure 8. Lagoon physical parameters of (a) water temperature (b) surface solar irradiance (c) salinity (d) and surface wind speed observed on JD 232. High and low water (blue lines) and non-daylight hours (grey areas) are also indicated.

426

427 **Table 3** Measured seawater salinity, temperature, pH and TA along with calculated DIC, pCO_2,
428 and air-sea CO_2 exchange rate (F_{GAS}) in the Inland Sea. The NEP value is the overall estimated
429 daytime average. A net carbon sink is inferred from a positive NEP value and a negative F_{GAS}
430 indicates a net transfer of CO_2 from the atmosphere to seawater. The mean water residence

time was derived from a validated 1-D MATLAB model of boundary volumetric flow, while DIC (± 8 µmol kg^{-1}) and pCO_2 (± 20 µatm) were derived from CO2Calc.

NEP (mmol C m^{-2} hr^{-1})	Mean Water Residence Time (hr)
3.0 ± 0.4	39 ± 6

Time (BST)	Salinity		Temp (°C)		pH_{sws}		TA (µmol kg^{-1})		DIC (µmol kg^{-1})		pCO2 (µatm)		F_{GAS} (mmol C m^{-2} hr^{-1})	
	JD213	JD232	JD213	JD232	JD213	JD232	JD213	JD232	JD213	JD232	JD213	JD232	JD213	JD232
08:00	33.3	34.0	17.5	16.6	8.04	8.12	2323	2329	2089	2055	406	325	0.022	-0.020
08:30	33.4	34.1	17.5	16.6	8.04	8.05	2323	2319	2089	2082	405	391	0.020	-0.002
09:00	33.4	34.0	17.5	16.6	8.04	8.05	2326	2329	2092	2092	406	394	0.016	-0.002
09:30	33.5	33.8	17.5	16.7	8.04	8.05	2325	2326	2090	2090	405	394	0.017	-0.002
10:00	33.4	33.8	17.5	16.9	8.04	8.07	2330	2317	2095	2070	407	371	0.022	-0.015
10:30	33.0	33.9	17.6	17.0	8.04	8.08	2333	2307	2100	2054	409	359	0.020	-0.026
11:00	33.3	34.1	17.8	17.1	8.06	8.13	2333	2303	2082	2020	385	312	-0.017	-0.061
11:30	33.3	34.0	18.0	17.3	8.09	8.13	2331	2302	2067	2019	355	312	-0.054	-0.076
12:00	33.3	34.0	18.3	17.5	8.08	8.13	2327	2307	2064	2021	364	312	-0.040	-0.080
12:30	33.5	33.9	18.7	17.7	8.08	8.11	2316	2306	2051	2031	362	330	-0.044	-0.072
13:00	33.6	33.9	19.1	17.9	8.11	8.12	2308	2302	2023	2020	331	321	-0.083	-0.113
13:30	33.6	34.0	19.6	18.1	8.12	8.12	2309	2303	2014	2018	322	320	-0.081	-0.109
14:00	33.6	34.0	19.9	18.4	8.12	8.15	2310	2304	2012	1999	322	294	-0.086	-0.147
14:30	33.6	33.8	20.2	18.8	8.13	8.15	2314	2301	2007	1994	313	294	-0.093	-0.185
15:00	33.4	33.9	20.5	19.1	8.16	8.18	2317	2304	1988	1976	288	270	-0.121	-0.242
15:30	33.6	33.8	20.5	19.5	8.16	8.17	2319	2300	1991	1975	288	277	-0.090	-0.236
16:00	33.6	33.9	20.7	19.6	8.21	8.17	2322	2302	1955	1975	249	277	-0.166	-0.229
16:30	33.7	34.0	20.3	19.6	8.18	8.21	2317	2299	1973	1946	271	246	-0.143	-0.318
17:00		34.1		19.5		8.17		2313		1984		278		-0.251
17:30		34.0		19.7		8.22		2308		1947		240		-0.298
18:00		34.0		19.5		8.19		2310		1970		263		-0.260
18:30		34.1		19.6		8.23		2308		1941		233		-0.357
19:00		34.1		19.6		8.24		2311		1937		227		-0.369
19:30		34.2		19.2		8.25		2317		1939		221		-0.380

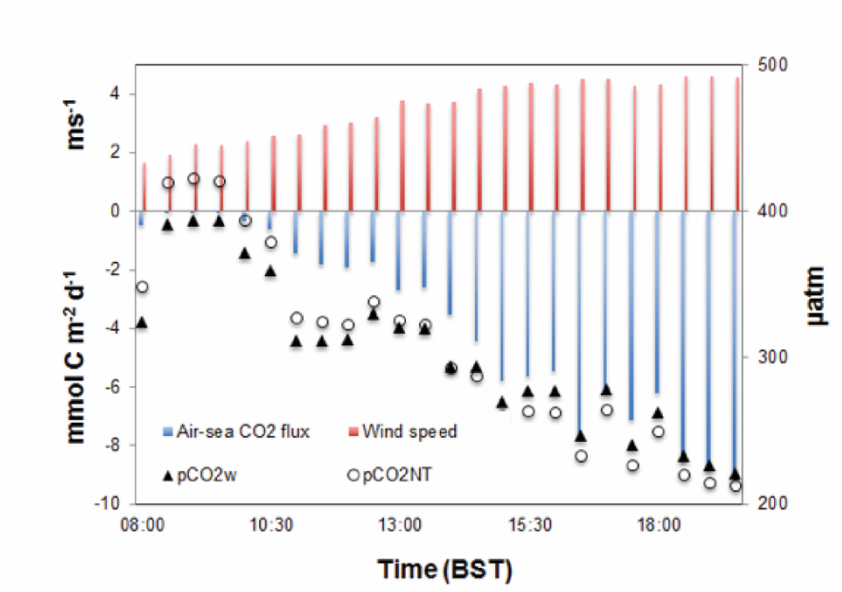

Figure 9. Air-sea CO_2 exchange, wind velocity, pCO_{2W} and temperature normalized partial pressure of CO_2, $pCO_{2,NT}$ for the study period on JD 232. Outgassing inferred from $pCO_{2,NT}$ values early in the study period is prevented by low water temperature that increases gas solubility and lowers pCO_{2W} preventing transfer of CO_2 from lagoon to atmosphere.

5. Discussion

5.1 Thermal effects

Temperature change affects the solubility of CO_2 in water, whereby an increase in temperature by 1°C causes approximately 4% pCO_{2W} increase as the dissolved gas dissociates (Gazeau et al., 2005; Jiang et al., 2011; De Carlo et al., 2013). Using CO2Calc to assess the maximum possible change of pCO_{2W} ($\Delta pCO_{2,T}$) from the temperature variation observed over the full tidal cycle on JD232 by fixing DIC and TA values at the lowest observed diel temperature and allowing pH to vary with inputs of minimum and maximum recorded temperature, we found that $\Delta pCO_{2,T}$ = 46 µatm. This is the maximum extent to which the temperature change within the lagoon can affect the pCO_{2W} of the system ($pCO_{2,T}$) during the study period. This value was confirmed by isolating the thermally forced pCO_{2W} changes to reveal only the change due to $pCO_{2,T}$ using the approach of Takahashi et al. (1993).

$$pCO_{2,T} = pCO_{2,mean} \times e^{0.0423 \times (Tobs - Tmean)} \quad (9)$$

Here $pCO_{2,T}$ and $pCO_{2,mean}$ are the pCO_{2W} values from thermal forcing alone and the in-situ average, respectively, while T_{mean} and T_{obs} are the in-situ mean and observed water temperature, respectively. This thermally isolated change reveals a similar 40 µatm change for the 3.2°C temperature increase observed in the lagoon water, resulting in only a 3.8% difference in value.

A maximum diel range in pCO_{2W} of approximately 172 µatm as observed on JD 232 (Figure 9) can be attributed to a combination of the remaining physical and biogeochemical processes within the lagoon, which have over three times the influence that temperature effects alone can explain. We used a similar approach in order to isolate the influences of the non-thermal processes of mixing, gas exchange and biological activity from the temperature effect on pCO_{2W} by normalizing to the mean temperature during empirical observations ($pCO_{2,NT}$) using the following formula:

$$pCO_{2,NT} = pCO_{2,Tobs} \times e^{0.0423\times(Tmean-Tobs)} \quad (10)$$

where $pCO_{2,NT}$ and $pCO_{2,Tobs}$ are the pCO_{2W} values from temperature normalized and actual observation calculations, respectively. The normalized values along with pCO_{2W} can be compared to reveal the time-based influence of temperature on the system.

The relative importance of thermal contribution over the course of the study period is highlighted by the lower temperatures in the lagoon at the start of the study due to low solar irradiance and the influence of incoming seawater. These factors promote greater solubility of CO_2 and act to prevent the system from outgassing to atmosphere during this time. As the day progresses and the absorbed radiant energy peaks, the thermal contribution predictably acts to increase pCO_{2W}. Given an assumed constant pCO_{2A} (396.7 ppm, NOAA, 2013), the air-sea flux drives CO_2 into the water column due to the increasing pCO_2 gradient, aided by an increase in wind velocity as the study period progressed, thus promoting aquatic CO_2 uptake (Takahashi et al., 2002). It should also be noted that the influence of processes acting to reduce pCO_{2W} appear to have greater impact in the lagoon than that of air-sea exchange influenced by wind speed (Figure 9).

Using CO2Calc (section 3.1) we compute pH_{25} from the recorded salinity, TA and DIC values (Table 3) and compare this with the in-situ pH data. As temperature has a significant impact on this parameter, the temperature corrected value highlights the biological influence in the signal. The corrected 25°C value is warmer than in-situ measurements, therefore we expect to see lower pH_{25} values. A clear reduction in the signal difference over time can be seen in Figure 10 as the lagoon system warms. The difference in the two pH values has a scale corrected range from 88.0% (08.30 to 09.00) to 93.4% (17.30) that can be attributed to biological activity alone.

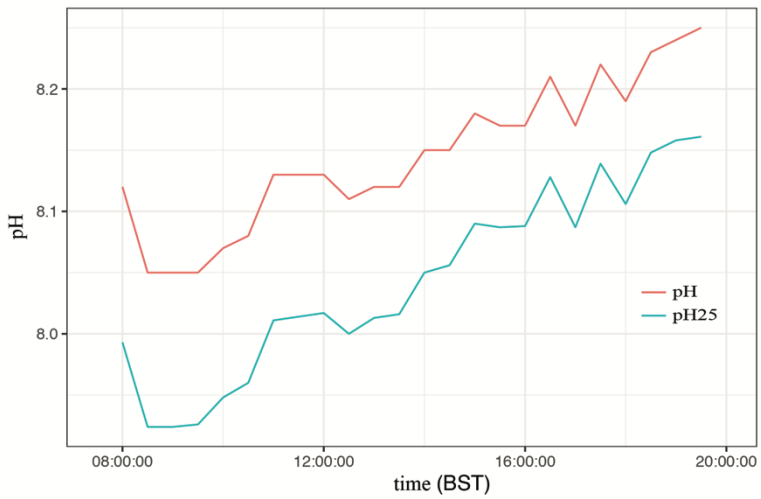

Figure 10. The pH_{25} was computed using CO2SYS from measured salinity, TA, and DIC values (Table 3), using a constant temperature of 25°C.

488

489 **5.2 Biogeochemical effects**

490 Using the stoichiometry of potential contributing biogeochemical processes that
491 could affect the CO_2 system of the lagoon, the fractional contribution of each to the TA-
492 DIC mass balance can be assessed. This is achieved by examining the distribution of
493 salinity-normalized values of lagoon TA against DIC concentration relative to the
494 equivalent incoming seawater concentration from outside the basin. Photosynthesis will
495 cause a slight increase in TA due to nutrient uptake and will reduce the DIC
496 concentration due to its uptake by primary producers within the system, whereas
497 respiration will have the opposite effect. Both processes result in a low ratio of TA to
498 DIC concentration change, with $\Delta A_T:\Delta C_T = -0.16$ (Lazar and Loya, 1991; Wolf-Gladrow
499 et al., 2007). The ratio of TA to DIC concentration change during calcification and
500 $CaCO_3$ dissolution is 2, while for benthic anaerobic respiration via sulphate reduction
501 with sulphide accumulation in sediment pore waters, $\Delta A_T:\Delta C_T = 1$ (Wang & Cai 2004;
502 Wolf-Gladrow et al., 2007; Soetaert et al., 2007; Zhai et al., 2017).

503 The dominance of each of these processes to the biogeochemistry of the
504 lagoon depends on a number of factors and could be overridden by external forces,
505 such as freshwater input, lagoon stratification, and water residence time (Gupta et al.,
506 2008; Kone et al., 2009; Muduli et al., 2012; Zhai et al., 2017). Their magnitude and
507 seasonal variability will affect the biogeochemistry of the lagoon and the net air-sea
508 CO_2 exchange. The trend in the current salinity-normalized TA versus DIC data over
509 the study period suggests that the carbonate system in the lagoon at full insolation was
510 influenced by photosynthesis and CO_2 transfer from the atmosphere (Figure 11). The
511 sustained increase of pH with temperature and stable TA throughout the heightened
512 solar period, combined with an increased air-sea flux gradient suggests that maximum
513 utilization of CO_2 occurs within the lagoon. Some moderate fluctuation in the normally
514 conservative TA parameter (Figure 7) suggests that it was affected somehow during

the study, but no water mass mixing occurs and $CaCO_3$ precipitation-dissolution appears to be negligible as a ΔA_T:ΔC_T = 2 in the salinity-normalized values would be expected (Figure 11).

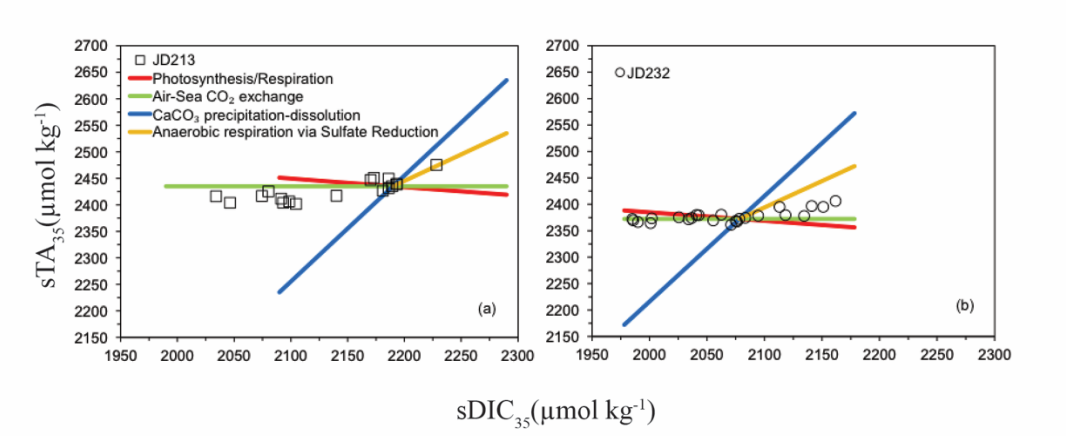

Figure 11. TA versus DIC concentrations in lagoon water observed during (a) JD 213 and (b) JD 232 normalized to S = 35, plotted relative to the inflowing seawater on each day. This is considered to be the baseline matrix altered by the physical-biogeochemical processes in the lagoon. The solid, colour coded lines indicate data distribution when individual physical-biogeochemical reactions dominate the carbonate system.

In studies of deeper coastal environments where only pelagic communities dominate, temperature drives short-term changes in the carbonate system (Dai et al., 2009). This study suggests that, in agreement with Jiang et al. (2011), within shallow nearshore systems, alterations driven by autotrophic benthic organisms may contribute most to ecosystem change.

5.3 Tidal influence

Overlaying the eularian carbonate system analyses during sampling periods highlights the tidal influence on the biological signal (Figure 12). The ebbing tide sampled on JD 213 exhibits a maximum lagoon DIC concentration of around 2090 µmol kg^{-1} at the start of observations (09.30) likely due to the overnight predominance of CR. The DIC concentration systematically decreases from that point throughout the day to around 1950 µmol kg^{-1} with an approximate linear trend of –20 µmol kg^{-1} hr^{-1} driven by autotrophic activity linked with increasing solar irradiance, which had a mean value of 580 ± 42 W m^{-2} (± 1s.d, n = 18) over the period.

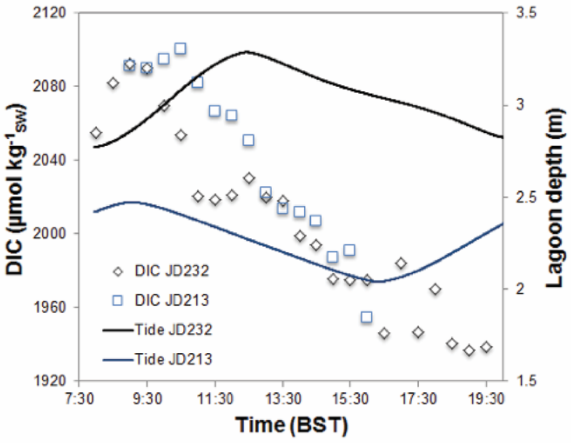

Figure 12. Lagoon tidal regime and observed inlet DIC concentration for both JD213 and JD232. A distinct pattern of diurnal biological production during the semi-diurnal tidal cycle fluctuation is present, indicating nutrient availability from tidal ebb and flood and daytime biology utilisation.

By comparison, during JD 232 when sampling started (08.00) on a flood tide, the DIC concentration within the lagoon initially increased from 2050 µmol kg^{-1} to 2090 µmol kg^{-1} due to a proportion of lagoon water that had earlier vacated the lagoon being forced back by the tide. Mixing of water carried back into the lagoon initially attenuates any biologically driven DIC concentration decrease. Net DIC loss becomes apparent after 09.30 when a sharp concentration drop was observed. The overall linear trend is approximately –13 µmol kg^{-1} hr^{-1} for a mean solar irradiance of 334 ± 35 W m^{-2} (± 1s.d, n = 25). As the sampling occurred during daylight hours, primary production appears to be the driver of DIC concentration change over time at this site. In contrast, community respiration would be expected to dominate at night (Frankignoulle and Bouquegneau, 1990) and during winter periods (Delille, Borges and Delille, 2009).

5.4 Diel NEP rate

The contribution of atmospheric carbon via CO_2 transfer from atmosphere to the lagoon during the sampling period was estimated to be 4.3% of NEP. Conceivably, this is as a direct result of the photosynthetic uptake in the Inland Sea. Jiang et al. (2011) and Muduli et al. (2013) report similar findings, with CO_2 transfer from the atmosphere playing a significant role in the latter study. In this study we determined a positive NEP of 3.0 ± 0.4 mmol C m^{-2} hr^{-1}, which indicates a net carbon sink due to primary production during daytime. This is the average ecosystem metabolism during the photic semi-diurnal period of study (12.12 hr). Therefore, approximately 96% of the daytime carbon NEP budget in the lagoon was supported by DIC availability from advected nutrients while the remainder came from surface interface atmospheric CO_2

559 transfer. The estimated time-integrated metabolic rate for the 13.5 hr total daylight
560 period is then equivalent to 40.5 ± 5.4 mmol C m^{-2}.
561 We lack site-specific information on CR, however, Hopkinson and Smith (2005)
562 report pelagic respiration rates in shallow inshore waters of between 58 and 114 mmol
563 C m^{-2} d^{-1}. Thus, assuming an overnight CR range of 2.42 – 4.75 mmol C m^{-2} hr^{-1} NEP
564 estimates during our study period would yield values between 15.23 and -9.24 mmol C
565 m^{-2} d^{-1}. Whereas using a CR value of 279 ± 184 mmol O_2 m^{-2} d^{-1} (*n* = 7) measured in *Z.*
566 *noltii* meadows in the Thau lagoon, France, and a photosynthetic quotient of 1 (Duarte
567 et al., 2010), a time-integrated CR of 122 ± 81 mmol C m^{-2} can be calculated over the
568 10.5 hr respiration-dominated night-time period. This then suggests a diel NEP rate of
569 approximately -82 ± 81 mmol C m^{-2} d^{-1} for our study site; the former range of estimates
570 being more consistent with the median NEP value of 20.6 mmol C m^{-2} d^{-1} reported in
571 seagrass ecosystem studies (Johnson et al., 2017).
572 Tokoro et al. (2014) presented global seagrass ecosystem NEP rates of 27 ± 6
573 mmol C m^{-2} d^{-1} converted from oxygen-based units. NEP estimates and errors may
574 vary dependent upon applied method and location. For example, Gazeau et al. (2005)
575 found that measured NEP rates fluctuated between 7 ± 1 mmol C m^{-2} d^{-1} and 41 ± 3
576 mmol C m^{-2} d^{-1}, with a mean of 22 ± 12 mmol C m^{-2} d^{-1}. Estimates of water residence
577 times, which are difficult to quantify in open embayment's, contributed most to
578 uncertainty. Ribas-Ribas et al. (2011) found NEP values between 10 and 60 mmol C m^{-2}
579 d^{-1} neglecting the influence of water residence time. Other studies have assessed
580 whether net autotrophic or heterotrophic behavior dominates in coastal systems based
581 on longer studies of NEP, estimated from rates of GPP and CR, with GPP known to
582 vary inter-annually by as much as 35% and NEP by 87% (Champenois and Borges,
583 2012).
584 The intertidal beds of the Inland Sea are colonized by the seagrass *Zostera*
585 *noltii*, which contribute to primary production in the study area. Papadimitriou et al.
586 (2006) estimated an increase in the above-ground seagrass biomass equivalent to 18
587 – 27 mmol C m^{-2} d^{-1} and in the below-ground biomass (roots and rhizomes) equivalent
588 to 22 – 28 mmol C m^{-2} d^{-1} during growth periods in spring and summer. Duarte et al.
589 (2005) reported on GPP, CR, and NEP for seagrass species and found that, in general,
590 seagrass meadows with GPP ≥ 180 mmol C m^{-2} d^{-1} were net autotrophic. Specifically,
591 for *Z. noltii*, ~66% of the meadows included in the Duarte et al. (2010) study had GPP
592 values of this magnitude, attesting to the potential for carbon sequestration for this
593 species of seagrass. Based on the limited daytime NEP data and assumed night-time
594 CR of Duarte et al. (2010), the seagrass community in our study site may be net
595 heterotrophic on an annual time scale but more detailed investigation is required to
596 validate this indication. Thus, future modelling of lagoon systems would benefit from

diurnal and seasonal sampling of the CO_2 system to obtain annual estimates of net carbon gain or loss to the atmosphere and to the adjacent Irish Sea waters.

5.5 Residence time

The box model approach utilized here allows us to quantify the input and output of CO_2 in the system from both advective lateral fluxes and surface transfer regimes, which is crucial in shallow nearshore ecosystems. However, it requires the ability to accurately predict water flow through the channels, because large uncertainties are introduced into calculations over short time scales (Borges et al., 2008). By considering an integrated approach over a tidal period, the uncertainty is somewhat attenuated. The integrated mean used to derive mass balance calculations are based on polynomial fits of the plotted observational data, with 95% confidence intervals of the standard deviation of the slope used to constrain NEP calculations.

Based on simplified unidirectional, unforced and hydrostatically balanced channel flow calculations ($0.5\ u^2 = -g\ d\eta/dx$) the contribution to error from uncertainty in harmonic boundary forcing in the MATLAB simulations causes a maximum elevation uncertainty of approximately 10 cm. This yields a maximum potential flow uncertainty of around 0.14 m s^{-1} in a channel of 100 m length (this error reduces for longer channels). However, validation data resolution was of the same order of magnitude, therefore this was ignored for NEP error estimate. The largest contribution to uncertainty for this study came from the estimated lagoon phase error of 0.11 ± 0.09 hr (n = 9). Assuming an average flow through the channel over the error phase period of 0.5 m s^{-1} (i.e. around slack water), a maximum difference in ΔF_{MIX} of approximately 0.15 mmol C m^{-2} Is possible. Therefore, greatest uncertainty is derived from the change in water residence time with phase shift. This results in an increase in the cumulative error estimation from ± 0.03 mmol C m^{-2} hr^{-1} to ± 0.4 mmol C m^{-2} hr^{-1} for a calculated difference in mean residence time of approximately 6 hours.

Based on a fixed tidal period and using the methods of this study, water residence time will increase if mean lagoon capacity increases or if the change in channel volumetric flow decreases (effectively a decrease in tidal range). An increase in residence time subsequently reduces NEP as the nutrients within the system take longer to be replenished and may result in a loss of seagrass habitat (Orfila et al., 2005). Delhez et al. (2014) report that the total time spent within the control domain may be significantly underestimated in oscillating flow regimes using the approach presented. It should be noted that calculation of residence time based on eq (6) utilizes the simple assumption that all of the water is exchanged through the channel, when in reality some of the water exiting or entering the lagoon returns immediately. A better approach may be to consider the fractional return of some of the water to avoid

635 overestimation of NEP (Sheldon and Alber, 2006; Rynne et al., 2016). Future work
636 should focus on constraining the parameters critical to estimating the time taken for
637 water to be replenished within the lagoon. Increased understanding of the lagoon
638 bathymetry, channel dimensions and substrate type would all conceivably contribute to
639 a reduction in modelled phase error.
640
641 **6. Conclusion**
642 Restricted lagoons such as the Inland Sea offer the ability to examine the
643 variation in NEP from DIC utilization and water residence period due to the nature of
644 their water exchange regimes. Increased high-resolution temporal monitoring using
645 autonomous techniques may be beneficial, as would constraining spatial distribution of
646 carbonate system concentrations. It has been shown that the overall net carbon
647 productivity of the Inland Sea ecosystem can be assessed over a complete tidal period
648 by conducting measurements of carbonate system parameters from water advected
649 through the channels, in combination with post observation, bulk parameterization
650 analysis. Development of methods should include autonomous measurements,
651 improved geophysical evaluation, enhanced validation and numerical hydrodynamic
652 modelling of boundary exchange, in order to further constrain estimates. Extrapolation
653 of calculated values for increased spatial and temporal assessment should also be a
654 future objective.
655 The overall net autotrophic balance of the seagrass containing system studied
656 suggests a potential sink for inorganic carbon during summer periods. An estimated
657 NEP of 40.5 ± 5.4 mmol C m^{-2} during the 13.5 hr daytime study period is equivalent to
658 a diel range of between 15.23 and -9.24 mmol C m^{-2} d^{-1} based on assumptions using
659 reported shallow water pelagic respiration rates. However, it is crucial to include
660 measurements of actual overnight respiration rate during studies, as a potential source
661 of inorganic carbon is calculated (-82 ± 81 mmol C m^{-2} d^{-1}) when literature values for
662 *Zostera noltii* meadows based on O_2 utilization is assumed. Furthermore, the former
663 approach suggests that approximately 4% of DIC is provided by CO_2 transfer from
664 atmosphere to ocean during the study period. Similar methodology may provide an
665 opportunity to assess the atmospheric carbon sequestration potential of planned
666 nearshore lagoon constructions. From the MRE perspective, there exists the potential
667 of enhancing the financial feasibility of tidal range lagoon energy schemes through
668 consideration of carbon offsetting. In particular when such structures are designed to
669 accommodate colonies of productive autotrophic flora.
670
671 **Acknowledgements**

With grateful thanks to Ben Butler and Charlotte Angove for the time, input, and support, they provided during fieldwork and in the laboratory for the duration of this project. The suggestion of using Hilbre Island weather station observatory data for solar irradiance values was kindly made by Madihah Jafar-Sidik and access granted by the Coastal Observatory at Liverpool bay (www.cobs.ac.uk). Meteorological information was accessed at weather underground (www.wunderground.com).

References

Auby I, and Labourg P J (1996) Seasonal Dynamics of *Zostera noltii* Hornem in the Bay of Arcachon (France). *Journal of Sea Research 35, 4*: 269-277.

Barnes R S K (1989) The Coastal Lagoons of Britain: An Overview and Conservation Appraisal. *Biological Conservation*: 295-313.

Barron C, Duarte C M, Frankignoulle M, and Borges A V (2006) Organic carbon metabolism and carbonate dynamics in a Mediterranean Seagrass (Posidonia oceanica) meadow. *Estuaries and Coasts* 29: 417–426.

Bauer J E, Cai W J, Raymond P A, Bianchi T S, Hopkinson C S, and Regnier P A G (2013) The changing carbon cycle of the coastal ocean. *Nature* 504, 7478: 61-70.

Borges A V, Delille B, and Frankignoulle M (2005) Budgeting sinks and sources of CO_2 in the coastal ocean: Diversity of ecosystems counts. *Geophysical Research Letters* 32: 1-4.

Borges A V, Ruddick K, Schiettecatte L S, and Delille B (2008) Net ecosystem production and carbon dioxide fluxes in the Scheldt estuarine plume. *BMC Ecology* 8, 15: 1-10.

Champenois W, and Borges A V (2012) Seasonal and interannual variations of community metabolism rates of a Posidonia oceanica seagrass meadow. *Limnology and Oceanography* 57, 1: 347–361.

Dai M, Lu Z, Zhai W, Chen B, Cao Z, Zhou K, Cai W J, and Chen C T A (2009) Diurnal variations of surface seawater pCO_2 in contrasting coastal environments. *Limnology and Oceanography* 54: 735-745.

De Carlo E H, Mousseau L, Passafiume O, Drupp P S, and Gattuso J P (2013) Carbonate Chemistry and Air-Sea CO2 Flux in a NW Mediterranean Bay Over a Four-Year Period: 2007-2011. *Aquatica Geochemica* 19: 399-442.

711 Delhez E J M, de Brye B, de Brauwere A, and Deleersnijder E (2014) Residence time vs
712 influence time. *Journal of Marine Systems* 132: 185-195.
713 http://dx.doi.org/10.1016/j.jmarsys.2013.12.005
714
715 Delille B, Borges A V and Delille D (2009) Influence of giant kelp beds (Macrocystis pyrifera)
716 on diel cycles of pCO_2 and DIC in the Sub-Antarctic coastal area. *Estuarine, Coastal and*
717 *Shelf Science* 81: 114-122.
718
719 Dickson A G, and Millero F J (1987) A comparison of the equilibrium constants for the
720 dissociation of carbonic acid in seawater media. *Deep Sea Research part A.*
721 *Oceanographic Research Papers* 34, 10: 1733-1743.
722
723 Dickson A G (1990) Standard potential of the reaction: AgCl(s) + ½H_2(g) = Ag(s) + HCl(aq),
724 and the standard acidity constant of the ion HSO_4^- in synthetic sea water from 273.15 to
725 318.15 K. *Journal of Chemical Thermodynamics* 22: 113-127.
726
727 Duarte C M, Middleburg J J, and Caraco N (2005) Major role of marine vegetation on the
728 oceanic carbon cycle. *Biogeosciences* 2: 1-8.
729
730 Duarte C M, Marbà N, Gacia E, Fourqurean J W, Beggins J, Barrón C, and Apostolaki E T
731 (2010) Seagrass community metabolism: Assessing the carbon sink capacity of seagrass
732 meadows. *Global Biogeochemical Cycles* 24: GB4032, doi:10.1029/2010GB003793.
733
734 Fourqurean J W, Duarte C M, Kennedy H, Marbà N, Holmer M, Mateo M A, Apostolaki E T,
735 Kendrick G A, Krause-Jensen D, McGlathery K J, and Serrano O (2012) Seagrass
736 ecosystems as a globally significant carbon stock. *Nature Geoscience*: 505-509. DOI:
737 10.1038/NGEO1477
738
739 Frankignoulle M, and Bouquegneau J M (1990) Daily and Yearly Variation of total Inorganic
740 Carbon in a Productive Coastal Area. *Estuarine, Coastal and Shelf Science* 30: 79-89.
741
742 Gazeau F, Duarte C M, Gattuso J P, Barron C, Navarro N, Ruiz S, Prairie Y T, Calleja M,
743 Delille B, Frankignoulle M, and Borges A V (2005) Whole-system metabolism and CO2
744 fluxes in a Mediterranean Bay dominated by seagrass beds (Palma Bay, NW
745 Mediterranean). *Biogeosciences* 2: 43-60.
746
747 Gleitz M, Rutgers van der Loeff M, Thomas D N, Dieckmann G S, and Millero F J (1995)
748 Comparison of summer and winter inorganic carbon, oxygen and nutrient concentrations in
749 Antarctic sea ice brines. *Marine Chemistry* 51**:** 81-91.
750
751 Goldman J C, and Brewer P G (1980) Effect of nitrogen source and growth rate on
752 phytoplankton-mediated changes in alkalinity. *Limnology Oceanography* 25: 352-357.

Gupta G V M, Sarma V V S S, Robin R S, Raman A V, Jai Kumar M, Rakesh M, and Subramanian B R (2008) Influence of net ecosystem metabolism in transferring riverine organic carbon to atmospheric CO2 in a tropical coastal lagoon (Chilka Lake, India). *Biogeochemistry* 87(3): 265-285.

Hill A E (1994) Fortnightly Tides in a Lagoon with Variable Choking. *Estuarine, Coastal and Shelf Science* 38: 423-434.

Hopkinson C S, and Smith E M (2005) Estuarine respiration: an overview of benthic, pelagic, and whole system respiration. *Respiration in Aquatic ecosystems* Chapter 8: 122-146. Oxford University Press DOI:10.1093/acprof:oso/9780198527084.003.0008

Jiang Z P, Huang J C, Dai M, Kao S J, Hydes D J, Chou W C, and Jan S (2011) Short-term dynamics of oxygen and carbon in productive nearshore shallow seawater systems of Taiwan: Observations and modelling. *Limnology and Oceanography* 56, 5: 1832-1849.

Johnson R A, Gulick A G, Bolten A B, and Bjorndal K A (2017) Blue carbon stores in tropical seagrass meadows maintained under green turtle grazing. *Nature: Scientific reports*: 7 13545. DOI:10.1038/s41598-017-13142-4

Kennedy H, and Bjork M (2009) Seagrass Meadows. In: Laffoley D, and Grimsditch G *The Management of Natural Coastal Carbon Sinks*: 23-29.

Kennedy H, Beggins J, Duarte C M, Fourqurean J W, Holmer M, Marbà N, and Middelburg J J (2010) Seagrass sediments as a global carbon sink: Isotopic constraints. *Global Biogeochemical Cycles* 24: 1-8.

Kjerfve B. (1986) Comparative Oceanography of Coastal lagoons. *Estuarine Variability*: 63-81.

Koné M, Abril G, Kouadio K N, Delille B, and Borges A (2009) Seasonal variability of carbon dioxide in the rivers and lagoons of Ivory Coast (West Africa). *Estuaries and Coasts* 32: 246-260. DOI: 10.1007/s12237-008-9121-0

Lazar B and Loya Y (1991) Bioerosion of coral reefs – A chemical approach. *Limnology and Oceanogr*aphy 36: 377-383.

Lee K, Kim T W, Byrne R H, Millero F J, Feely R A, and Liu Y M (2010) The universal ratio of boron to chlorinity for the North Pacific and North Atlantic oceans. *Geochemica et Cosmochimica Acta* 74, 6: 1801-1811.

Le Quéré C, Andres R J, Boden T, Conway T, Houghton R A, House J I, Marland G, Peters G P, van der Werf G R, Ahlström A, Andrew R M, Bopp L, Canadell J G, Ciais P, Doney S C, Enright C, Friedlingstein P, Huntingford C, Jain A K, Jourdain C, Kato E, Keeling R F, Klein Goldewijk K, Levis S, Levy P, Lomas M, Poulter B, Raupach M R, Schwinger J, Sitch S, Stocker B D, Viovy N, Zaehle S, and Zeng N (2013) The global carbon budget 1959–2011. *Earth System Science Data* 5, 1: 165-185. https://doi.org/10.5194/essd-5-165-2013.

Le Quéré, C., Andrew, R. M., Friedlingstein, P., Sitch, S., Pongratz, J., Manning, A. C., Korsbakken, J. I., Peters, G. P., Canadell, J. G., Jackson, R. B., Boden, T. A., Tans, P. P., Andrews, O. D., Arora, V. K., Bakker, D. C. E., Barbero, L., Becker, M., Betts, R. A., Bopp, L., Chevallier, F., Chini, L. P., Ciais, P., Cosca, C. E., Cross, J., Currie, K., Gasser, T., Harris, I., Hauck, J., Haverd, V., Houghton, R. A., Hunt, C. W., Hurtt, G., Ilyina, T., Jain, A. K., Kato, E., Kautz, M., Keeling, R. F., Klein Goldewijk, K., Körtzinger, A., Landschützer, P., Lefèvre, N., Lenton, A., Lienert, S., Lima, I., Lombardozzi, D., Metzl, N., Millero, F., Monteiro, P. M. S., Munro, D. R., Nabel, J. E. M. S., Nakaoka, S.-I., Nojiri, Y., Padin, X. A., Peregon, A., Pfeil, B., Pierrot, D., Poulter, B., Rehder, G., Reimer, J., Rödenbeck, C., Schwinger, J., Séférian, R., Skjelvan, I., Stocker, B. D., Tian, H., Tilbrook, B., Tubiello, F. N., van der Laan-Luijkx, I. T., van der Werf, G. R., van Heuven, S., Viovy, N., Vuichard, N., Walker, A. P., Watson, A. J., Wiltshire, A. J., Zaehle, S., and Zhu, D. (2018) Global Carbon Budget 2017. *Earth Syst. Sci. Data 10*, 405-448, https://doi.org/10.5194/essd-10-405-2018.

Mehrbach C, Pytkowicz R M, Hawley J, Culberson C, and Barton B (1973) Measurements of the apparent dissociation constants of carbonic acid in seawater at atmospheric pressure. *MSc Thesis, Oregon State University, Corvallis*: Suelyn Williams.

Mørk E T, Sejr M K, Stæhr P A, and Sørensen L L (2016) Temporal variability of air-sea CO2 exchange in a low-emission estuary. *Estuarine, Coastal and Shelf Science* 176: 1-11.

Muduli P, Kanuri V V, Robin R S, Charan Kumar B, Patra S, Raman A V, Nageswarara Rao G, and Subramanian B R (2012) Spatio-temporal variation of CO2 emission from Chilka Lake, a tropical coastal lagoon on the east coast of India. *Estuarine, Coastal and Shelf Science* 113: 305-313.

Muduli P, Kanuri V V, Robin R S, Charan Kumar B, Patra S, Raman A V, Nageswarara Rao G, and Subramanian B R (2013) Distribution of dissolved inorganic carbon and net ecosystem production in a tropical brackish water lagoon, India. *Continental Shelf Research* 64: 75-87.

Neill S, Angeloudis A, Robins P, Walkington I, Ward S, Masters I, Lewis M, Piano M, Avdis A, Piggott M, Aggidis G A, Evans P, Adcock T, Zidonis A, Ahmadian R, and Falconer R (2018) Tidal range energy resource and optimization – past perspectives and future challenges. *Renewable Energy* 127: 763-778. DOI: 10.1016/j.renene.2018.05.007

Newton A, and Mudge S M (2005) Lagoon-sea exchanges, nutrient dynamics and water quality management of the Ria Formosa (Portugal). *Estuarine, Coastal and Shelf Science* 62, 3: 405-414.

NIC (National Infrastructure Commission) *National Infrastructure Assessment technical annex: Tidal power* (accessed Aug 8th, 2018) https://www.nic.org.uk/wp-content/uploads/Tidal-power.pdf

NOAA (National Oceanic and Atmospheric Administration) *Trends in atmospheric carbon dioxide* (accessed Aug 31st, 2013) http://www.esrl.noaa.gov/gmd/ccgg/trends/global.html

Orfila A, Jordi A, Basterretxea G, Vizoso G, Marba N, Duarte C M, Werner F E, and Tintor Ã J (2005) Residence time and Posidonia oceanica in Cabrera Archipelago National Park, Spain. *Continental Shelf Research* 25: 1339-1352 10.1016/j.csr.2005.01.004.

Papadimitriou S, Kennedy H, Rodrigues R M, Kennedy D P, and Heaton T H (2006) Using variation in the chemical and stable isotopic composition of Zostera noltii to assess nutrient dynamics in a temperate seagrass meadow. *Organic chemistry* 37: 1343-1358.

Papadimitriou S, Kennedy H A, Norman L, Kennedy D P, Dieckmann G S, and Thomas D N (2012) The effect of biological activity, CaCO3 mineral dynamics, and CO2 degassing in the inorganic carbon cycle in sea ice in late winter-early spring in the Weddell Sea, Antarctica. *Journal of Geophysical Research* 117: 1-12.

Ribas-ribas M, Hernández-Ayón J M, Camacho-Ibar V F, Cabello-Pasini A, Mejia-Trejo A, Durazo R, Galindo-Bect S, Souza A J, Forja J M, and Siqueiros-Valencia A (2011) Effects of upwelling, tides and biological processes on the inorganic carbon system of a coastal lagoon in Baja California. *Estuarine, Coastal and Shelf Science* 95: 367-376.

Robbins L L, Hansen M E, Kleypas J A, and Meylan S C (2010) CO2calc: A user-friendly seawater carbon calculator for Windows, Mac OS X, and iOS (iPhone). U.S. Geological Survey, 17.

Roche R C, Walker-Springett K, Robins P E, Jones J, Veneruso G, Whitton T A, Piano M, Ward S L, Duce C E, Waggitt J J, Walker-Springett G R, Neill S P, Lewis M J, and King J W (2016) Research priorities for assessing potential impacts of emerging marine renewable energy technologies: Insights from developments in Wales (UK). *Renewable Energy* 99: 1327-1341.

877 Rynne P, Reniers A, van de Kreeke J, and Macmahan J (2016) The effect of tidal exchange
878 on residence time in a coastal embayment. *Estuarine, Coastal and Shelf Science* 172.
879 10.1016/j.ecss.2016.02.001.
880
881 Sheldon J E, and Alber M (2006) The calculation of estuarine turnover times using
882 freshwater fraction and tidal prism models: A critical evaluation. *Estuaries and Coasts* 29, 1:
883 133-146.
884
885 Soetaert K, Hofmann A F, Middelburg J J, Meysman F J R, and Greenwodd J (2007) The
886 effect of biogeochemical processes on pH. *Marine Chemistry* 105: 30-51.
887
888 Takahashi T, Olafsson J, Goddard J G, Chipman D W, and Sutherland S C (1993)
889 Seasonal Variations of CO2 and Nutrients in the High Latitude Surface Ocean: A
890 Comparative study. *Global Biogeochemical Cycles* 7: 843-878.
891
892 Takahashi T, Sutherland S C, Sweeney C, Poisson A, Metzl N, Tilbrook B, Bates N,
893 Wanninkhof R, Feely R A, Sabine C, Olafsson J, and Nojiri Y (2002) Global sea–air CO2
894 flux based on climatological surface ocean pCO2, and seasonal biological and temperature
895 effects. *Deep Sea Research Part II Topical Studies in Oceanography* 49: 1601-1622.
896 https://doi.org/10.1016/S0967-0645(02)00003-6
897
898 Tokoro T, Hosokawa S, Miyoshi E, Tada K, Watanabe K, Montani S, Kayanne H, and
899 Kuwae T (2014) Net uptake of atmospheric CO_2 by coastal submerged aquatic vegetation.
900 *Global Change Biology* 20(6): 1873-1884 doi: 10.1111/gcb.12543
901
902 Tsihrintzis V A, Sylaios G K, Sidiropoulou M, and Koutrakis E T (2007) Hydrodynamic
903 modeling and management alternatives in a Mediterranean, fishery exploited, coastal
904 lagoon. *Aquacultural Engineering* 36: 310-324.
905
906 Wang Z A, and Cai W J (2004) Carbon dioxide degassing and inorganic carbon export from
907 a marsh-dominated estuary (the Duplin River): A marsh CO_2 pump. *Limnol. Oceanogr.*
908 49(2), 341–354. http://dx.doi.org/10.4319/lo.2004.49.2.0341.
909
910 Wanninkhof R (1992) Relationship between wind speed and gas exchange over the ocean.
911 *Journal of Geophysical Research* 97, C5: 7373-7382.
912
913 Williams R G, and Fellows M J (2011) *Ocean Dynamics and the Carbon Cycle: Principles*
914 *and Mechanisms.* New York: Cambridge University Press.
915
916 Wolf-Gladrow D A, Zeebe R E, Klaas C, Körtzinger A, and Dickson A G (2007) Total
917 alkalinity: The explicit conservative expression and its application to biogeochemical
918 processes. *Marine Chemistry* 106: 287-300.

Zhai W D, Yan X L, and Qi D (2017) Biogeochemical generation of dissolved inorganic carbon and nitrogen in the North Branch of inner Changjiang Estuary in a dry season. *Estuarine, Coastal and Shelf Science* 197:136-149. DOI: http://dx.doi.org/10.1016/j.ecss.2017.08.027.

Zouiten H, Diaz C A, Gomez A G, Cortezon J A R, and Alba J C (2013) An advanced tool for eutrophication modeling in coastal lagoons: Application to the Victoria lagoon in the north of Spain. *Ecological Modelling* 265: 99-113.

Tables and Figures[+]

[+]*Colour to be used for Figures except 2, 3 and 5.*